EPJ manuscript No.
(will be inserted by the editor)

Cluster transfer reactions with the combined R-matrix and Lagrange-mesh methods

A Tribute to Mahir Hussein

Shubhchintak[1]

Physique Nucléaire Théorique et Physique Mathématique, C. P. 229, Université Libre de Bruxelles (ULB), B 1050, Brussels, Belgium

Received: date / Revised version: date

Abstract. We have recently applied the R-matrix method to transfer reactions in the distorted wave Born approximation (DWBA) framework. In our approach the wave function in the internal region is expanded in terms of Lagrange basis, which provides a fast and efficient way to compute the matrix elements. This paper is a short review of our work on transfer reactions. I discuss applications of our approach by considering the ^{16}O$(d,n)^{17}$F and ^{12}C(^{7}Li, $t)^{16}$O reactions, which are specific examples of neutron and α transfer, respectively. In particular, I discuss the role of the remnant terms, post-prior form equivalence, peripherality of the reaction and sensitivity of the transfer cross sections to the bound state wave functions. Effects of the remnant terms and of the supersymmetric bound state potentials on the extracted spectroscopic factors are also discussed.

PACS. XX.XX.XX No PACS code given

1 Introduction

A nuclear cluster can be defined as a subsystem of strongly correlated nucleons having its intrinsic binding stronger than the external binding [1]. Similar to the nucleons, clusters are also considered to have their specific orbitals and more often they are treated as a single entity without reference to their internal structure. A well-known example is the α cluster which consists of two protons and two neutrons and has high binding energy. Other clusters such as tritions and helions are also common. On the basis of several studies, it is now established that these kind of structures are more plausible on the nuclear surface and therefore can easily participate in various nuclear reactions.

Mahir Saleh Hussein was a great expert of the nuclear reaction theory and in his professional life he has worked on various types of nuclear reactions. In this short review, I focus on the role of nuclear transfer reactions to the nuclear structure study, the area where Mahir Hussein has also contributed significantly (see for example[2–4]). In fact, nuclear reactions involving the transfer of nucleon(s) or clusters among the projectile and target, provide a powerful spectroscopic tool to probe the nuclear surface and hence to understand the single particle or cluster character of nuclear states [5–8]. This is due to the sensitivity of transfer cross sections to the structure of the projectile and the residual nucleus (composite formed by the transferred cluster and the target). In particular, comparing the measured angular distribution of the cross sections with the calculated ones, the angular momentum (ℓ) and the spin-parity (J^π) of a particular residual state can be figured out. With the same procedure one can also find out the spectroscopic factor (SF) or the asymptotic normalization coefficients (ANC) (defined as the amplitude of the tail of the overlap function) of the participating state of residual nucleus. These information are important to further specify their single particle or the cluster structure. In case the final state is a resonance, one can estimate the width of the resonance by knowing the SF or the ANC. For example, in Ref. [9], role of the ANC in determining the radiative width was discussed. Apart from the structure studies, such information (like energies, widths, spin etc.) are often desired in many important astrophysical reactions.

In fact, transfer reactions provide an indirect way to study the astrophysical reactions when at low energies it becomes difficult to perform direct measurements [10–12]. For example, in Ref. [13], the ^{16}O(^{3}He, $d)^{17}$F reaction was measured to analyze the states of ^{17}F and the deduced ANCs were then used to determine the low energy radiative capture cross sections of the ^{16}O(p, $\gamma)^{17}$F reaction. Similarly, the cluster transfer reactions such as (^{6}Li, d) and (^{7}Li, t), where an α cluster transfer from the projectile to the target, have been used to study the important

Send offprint requests to: Shubhchintak
Correspondence to: shubhchintak@ulb.ac.be

astrophysical reactions like ^{12}C$(\alpha,\gamma)^{16}$O, ^{13}C$(\alpha,n)^{16}$O, ^{22}Ne$(\alpha,\gamma)^{26}$Mg, (for details see for example the review article [10]). It is now well established that cross sections of low energy peripheral radiative capture reactions are mainly determine by the ANCs. Some recent studies are focused in extracting the (n,γ) cross sections for the r process nuclei using (d,p) reactions [4,14,15].

At the simplest, without referring to the internal structures of the transferred cluster, core of the projectile and the target, one can consider transfer as a three-body reaction. Therefore, the same approach can be used for the single particle as well as for the cluster transfer reactions and with this picture several theoretical models using different frameworks and approximations have been developed in the literature. The standard and the most widely used framework is the 'distorted wave Born approximation (DWBA)' [5]. In this approximation the transfer is considered as one-step process, weak enough to be treated as a first order perturbation. Other methods such as the adiabatic method [16], the continuum discretized coupled-channel (CDCC) method [17] and the Faddeev method [18,19] are more advanced than standard DWBA. Among these, the Faddeev method uses the exact three-body wave function while the adiabatic and the CDCC methods approximate it better than the DWBA by including breakup effects. For a comparison of these methods one can see, for example, Refs. [17,20,21]

Modern calculations, like those in the CDCC method, are demanding in terms of computer capabilities. The availability of efficient numerical techniques is therefore an important issue. As a first step in this direction, in Refs. [22, 23] we have applied the combined R-matrix [24,25] and the Lagrange mesh [26] methods, to the transfer reaction study in the DWBA frame work. Apart from simplifying the calculations, usage of these methods lead to fast and accurate numerical computations.

This paper is a short review of our work on transfer reactions, where apart from the utility of the R-matrix and the Lagrange mesh methods, I also discuss about the sensitivity of the transfer cross sections to the bound state wave functions [23]. For this, a supersymmetric bound state partner of the Woods-Saxon potential is used, which gives a different wave function in the nuclear interior but have the same asymptotics. Comparing the calculated cross section with the data for reactions under consideration, changes in the SFs are estimated. As mentioned earlier, the same framework can be used for the nucleon as well as for the cluster transfer reactions, so here I consider one example for each of them. In particular, I consider the ^{16}O$(d,n)^{17}$F and the ^{12}C$(^7$Li, $t)^{16}$O reactions which are the specific examples of proton and of α transfer, respectively. The latter reaction we have studied in Refs. [22,23] along with the ^{16}O$(d,p)^{17}$O, but our results for the former have not been presented before.

The paper is organized as follows. In section 2, I present the DWBA formalism of transfer reactions and also discuss in brief about the R-matrix and the Lagrange mesh methods. Section 3 consists of results and discussion and finally I summarize in section 4.

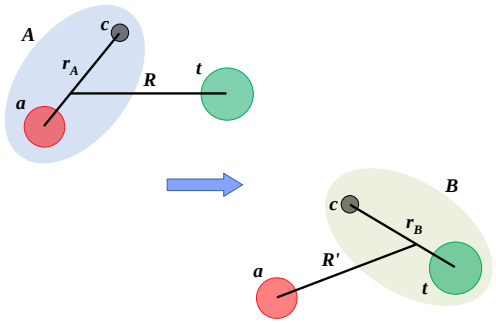

Fig. 1. Schematic diagram of transfer process where a cluster c is transferred from the projectile A to the target t. The angles Ω and Ω' are associated with the coordinates R and R'.

2 Formalism

2.1 DWBA theory of transfer reactions

I give here brief details of the DWBA formalism, which of course has been discussed in many textbooks and reviews [5–8,27]. For more details about the current approach one is referred to [22]. We consider a projectile A which transfers a cluster/nucleon c to the target t (spin-less in our case) leading to the formation of a residual nucleus B and an outgoing core a in the final channel. This rearrangement reaction can be written as

$$A(=a+c)+t\rightarrow B(=t+c)+a. \tag{1}$$

Fig. 1 displays the various coordinates involved in the above process. The three-body Hamiltonian associated with this transfer process (1) can be defined in the "prior" representation [5,6] as

$$H_{\rm prior}=H_A(\boldsymbol{r}_A)+T_{\boldsymbol{R}}+V_{ct}(\boldsymbol{r}_B)+U_{at}(\boldsymbol{r}_{at}), \tag{2}$$

or, in the "post" representation, as

$$H_{\rm post}=H_B(\boldsymbol{r}_B)+T_{\boldsymbol{R'}}+V_{ac}(\boldsymbol{r}_A)+U_{at}(\boldsymbol{r}_{at}), \tag{3}$$

where V_{ij} are the binding potentials between clusters i and j and they are generally obtained by fitting the spectroscopic properties such as binding energies or root-mean-square radii. U_{at} is the optical potential between a and t which is generally fitted to the elastic scattering data and is also called core-core potential. $\boldsymbol{r}_{at}$ is the distance between particles a and t. H_A and H_B are the internal Hamiltonians of nuclei A and B, respectively and in the two-body model they are given by

$$\begin{aligned} H_A&=T_A+V_{ac}(\boldsymbol{r}_A),\\ H_B&=T_B+V_{ct}(\boldsymbol{r}_B). \end{aligned} \tag{4}$$

The two-body bound state wave functions for nuclei A and B with their respective Hamiltonians are given by

$$\begin{aligned} \Phi^{I_AM_A}_{\ell_A}(\boldsymbol{r}_A)&=\frac{1}{r_A}u^{I_A}_{\ell_A}(r_A)\Big[Y_{\ell_A}(\Omega_A)\otimes\big[\chi_a\otimes\chi_c\big]^{S_A}\Big]^{I_AM_A},\\ \Phi^{I_BM_B}_{\ell_B}(\boldsymbol{r}_B)&=\frac{1}{r_B}u^{I_B}_{\ell_B}(r_B)\big[Y_{\ell_B}(\Omega_B)\otimes\chi_c\big]^{I_BM_B}, \end{aligned} \tag{5}$$

where $u^{I_k}_{\ell_k}$ is the radial bound state wave function of the nucleus k with ℓ_k and I_k are its orbital angular momentum (the parity is implied) and spin, respectively. χ_j is the spinor associated with the particle j. As mentioned earlier, we have consider the target with zero spin and further we assume that it cannot be excited. A generalization can be found in Ref. [28].

The post and the prior representations [Eqs. (2, 3)] in the DWBA are known to be strictly equivalent (also true when the exact wave function is used) and in the literature one can find the merits of both choices (for example, see Refs. [29,30]). For the purpose of this paper I use the post representation, but the developments are similar for the prior representation and we have verified their equivalence in all our calculations which I shall also discuss in next section.

Considering $U_\delta(\boldsymbol{R}')$ as some auxiliary potential between nuclei a and B, the asymptotic Hamiltonian in the final channel can be written as

$$H_\beta = H_B(\boldsymbol{r}_B) + T_{\boldsymbol{R}'} + U_\delta(\boldsymbol{R}'). \tag{6}$$

The wave function, for the above Hamiltonian then can be factorized as

$$\Phi^{JM\pi(-)}_\beta(\boldsymbol{r}_B, \boldsymbol{R}') = \frac{\chi^{J\pi}_{L_B}(R')}{R'}\left[Y_{L_B}(\Omega') \otimes \left[\Phi^{I_B}_{\ell_B}(\boldsymbol{r}_B) \otimes \chi_a\right]^{S_B}\right]^{JM}, \tag{7}$$

where J, π stands for the total angular momentum and parity, respectively and the orbital angular momentum in the exit channel is represented by L_B. $\chi^{J\pi}_{L_B}(R')$ is the radial scattering wave function for the relative motion of a and B which is generated by the $a + B$ optical potential. Note that, in our calculations all optical potentials are considered as local. Furthermore, in DWBA, the choice of the auxiliary potential U_δ is not arbitrary [29] and in this case it as U_{aB} i.e. the optical potential between a and B.

If we consider $\Psi^{JM\pi(+)}_\alpha(\boldsymbol{r}_A, \boldsymbol{R})$ as the exact three-body solution in the initial channel then the scattering matrix $U^{J\pi}_{\alpha\beta}$ for the transfer process can be defined as

$$U^{J\pi}_{\alpha\beta} = -\frac{i}{\hbar}\langle \Phi^{JM\pi(-)}_\beta | V_{ac} + U_{at} - U_{aB} | \Psi^{JM\pi(+)}_\alpha \rangle, \tag{8}$$

where labels α and β stand for (L_A, ℓ_A, I_A) and (L_B, ℓ_B, I_B), respectively.

In the DWBA, the exact three-body wave function $\Psi^{JM\pi(+)}_\alpha$ can be approximated as

$$\Psi^{JM\pi(+)}_\alpha(\boldsymbol{r}_A, \boldsymbol{R}) \approx \frac{\chi^{J\pi}_{L_A}(R)}{R}\left[Y_{L_A}(\Omega) \otimes \Phi^{I_A}_{\ell_A}(\boldsymbol{r}_A)\right]^{JM}, \tag{9}$$

where $\chi^{J\pi}_{L_A}(R)$ is the radial scattering wave function for the relative motion of A and t. Wave functions in Eq. (7) and Eq. (9) are therefore treated on an equal footing.

Substituting these equations [(7) and (9)] into Eq. (8), the DWBA scattering matrix element can be simplified as

$$U^{J\pi}_{\alpha\beta} = -\frac{i\sqrt{SF_A SF_B}}{\hbar} \times \int \chi^{J\pi}_{L_A}(R) K^{J\pi}_{\alpha\beta}(R, R') \chi^{J\pi}_{L_B}(R') R R' dR dR', \tag{10}$$

where SF_A and SF_B are the spectroscopic factors of the concerned bound states of nucleus A and nucleus B, respectively. $K^{J\pi}_{\alpha\beta}(R, R')$ is the transfer kernel, which is given by

$$K^{J\pi}_{\alpha\beta}(R, R') = \mathcal{J}\langle \left[Y_{L_A}(\Omega) \otimes \Phi^{I_A}_{\ell_A}(\boldsymbol{r}_A)\right]^J | \mathcal{V} | \left[Y_{L_B}(\Omega') \otimes \Phi^{I_B}_{\ell_B}(\boldsymbol{r}_B)\right]^J \rangle. \tag{11}$$

In the above equation, $\mathcal{J} = [\frac{m_A\, m_B}{m_c(m_A+m_t)}]^3$ (m_i is the mass of particle i) is the Jacobian [22] which is introduced to take care of transformations from the natural sets of independent variables $(\boldsymbol{R}, \boldsymbol{r}_A)$, $(\boldsymbol{R}', \boldsymbol{r}_B)$ to the set $(\boldsymbol{R}, \boldsymbol{R}')$ which is usually adopted for symmetry reasons. Calculation of the transfer kernel [Eq. (11)] involves integral over the angles Ω and Ω' and they were given in the Appendix or Ref. [22]. The interaction $\mathcal{V}$ in Eq. (11), in the post form is given by

$$\mathcal{V}_{post} = V_{ac} + U_{at} - U_{aB}. \tag{12}$$

Similar procedure if followed for the prior form, then one can get the equivalent expression for the scattering matrix [Eq. (10)], but the interaction $\mathcal{V}$ in that case will be

$$\mathcal{V}_{prior} = V_{ct} + U_{at} - U_{At}. \tag{13}$$

In both these representations, the latter two terms (also called remnant terms) are often neglected for the simplicity as they appear nearly equal in many cases. However, this is true when target t is heavy in the post representation or when core a and target t are heavier than the transferred cluster in the prior representation. For example, in the case of (d, p) reactions in post form, optical potentials for the $p - \mathrm{A}_t$ and $p - (\mathrm{A}_t + 1)$ (A_t being the mass number of the target) systems appear nearly same and their difference can be neglected. On the other hand, in the prior form the remnant term involves optical potentials for the $p - \mathrm{A}_t$ and $d - \mathrm{A}_t$ systems and their difference generally can't be neglected. This is also one of the reasons that in the literature, for the (d, p) reactions, the post form DWBA is mostly used without the remnant term in the interaction. Also note that the equivalence of these two representations hold only when remnant terms are included in the calculations [31].

The evaluation of Eq. (10) needs scattering wave functions in the incident as well as in the exit channels along with the bound state functions. For this, we make use of the R-matrix and the Lagrange mesh methods, which I discuss in brief in the next section.

2.2 R-matrix and Lagrange mesh methods

For a detailed review of the R-matrix method and its applications one is referred to Ref. [24], here I shall discuss only what is relevant in the present context. We use this method to calculate the scattering wave functions $\chi^{J\pi}_{L_A}(R)$ and $\chi^{J\pi}_{L_B}(R')$. Following the idea of the R-matrix, we divide the space in an internal and an external region at

some radius R_0. The channel radius R_0 is taken large enough, so that, beyond this the nuclear potential is negligible. In the external region ($R > R_0$), the wave function take the asymptotic form, which is given by

$$\chi^L_{\rm ext}(R) = \frac{1}{\sqrt{v}}(I_L(kR) - U_L O_L(kR)), \tag{14}$$

where k and v respectively are the wave numbers and velocity of the concerned particle. $I_L(x)$ and $O_L(x)$ are the incoming and outgoing Coulomb functions, respectively and U_L is the elastic scattering matrix which is calculated from the R-matrix. Note that, for the simplicity, in this section I have dropped the dependency of the wave function on other indices except the orbital angular momentum.

In the internal region ($R \leq R_0$), the wave function is expanded over a set of N basis functions $\varphi_i(R)$ as

$$\chi^L_{int}(R) = \sum_{i=1}^{N} c^L_i \varphi_i(R). \tag{15}$$

The choice of the basis functions $\varphi_i(R)$ will be discussed later. These functions are valid only in the region $[0, R_0]$, therefore the matrix elements of the kinetic energy are not Hermitian. This problem can be solved by introducing the Bloch operator [32], defined as

$$\mathcal{L} = \frac{\hbar^2}{2\mu}\delta(R - R_0)\left(\frac{d}{dR} - \frac{B}{R}\right), \tag{16}$$

with B as a boundary parameter, taken as 0 here and μ is the reduced mass. The Bloch-Schrödinger equation can be written as

$$\big(H + \mathcal{L} - E\big)\chi^L_{\rm int} = \mathcal{L}\chi^L_{\rm int} = \mathcal{L}\chi^L_{\rm ext}, \tag{17}$$

where the second equality holds because of the surface character of $\mathcal{L}$. Note that apart from ensuring the hermiticity of the Hamiltonian over the internal region the Bloch operator also leads to the continuity of the derivative at the boundary .i.e. ${\chi^L_{\rm int}}'(R_0) = {\chi^L_{\rm ext}}'(R_0)$.

By substituting Eq. (15) into Eq. (17) one can calculate the expansion coefficients c^L_i, which are given by

$$c^L_i = \sum_j (C^{-1}_L)_{ij}\langle\varphi_j|\mathcal{L}|\chi^L_{\rm ext}\rangle, \tag{18}$$

with matrix $\boldsymbol{C}_L$ as

$$\big(\boldsymbol{C}_L\big)_{ij} = \langle\varphi_i|H + \mathcal{L} - E|\varphi_j\rangle. \tag{19}$$

The R-matrix (R_L) which is defined as the reciprocal of the logarithmic derivative of the wave function at the channel radius R_0, is then given by

$$R_L = \frac{\hbar^2}{2\mu R_0}\sum_{ij}\varphi_i(R_0)\big(\boldsymbol{C}^{-1}_L\big)_{ij}\varphi_j(R_0). \tag{20}$$

Using the continuity condition $\chi^L_{\rm int}(R_0) = \chi^L_{\rm ext}(R_0)$, the elastic scattering matrix U_L can be calculated as

$$U_L = \frac{I_L(kR_0)}{O_L(kR_0)}\frac{1 - \mathbb{L}^*\,R_L}{1 - \mathbb{L}\,R_L}, \tag{21}$$

where constant $\mathbb{L}$ is defined as

$$\mathbb{L} = ka\frac{O'_L(ka)}{O_L(ka)}. \tag{22}$$

At this point, it is worth mentioning that the channel radius R_0 is not a parameter here and the scattering matrix U_L should not depend on it even though the R-matrix and Coulomb functions do. It is selected to be large enough so that the nuclear interaction becomes negligible. But on the other hand large channel radius require a large number of basis functions $\varphi_i(R)$ which increase the computer times. So to compromise here, one is recommended to choose the channel radius as small as possible (provided that the nuclear interactions become negligible).

In our calculations, the basis functions $\varphi_i(R)$ are chosen as Lagrange functions. These are N infinitely differentiable functions, which form an orthonormal set and they vanish at all mesh points except one. The other important property of these functions is the associated Gauss quadrature. For more details about this method and about the accuracy of the Gauss approximation, one is referred to [26].

The choice of these functions depends on the interval considered. For a finite interval $[0, R_0]$ as in our case for the R-matrix procedure, the N Lagrange functions are chosen as [24,22]

$$\varphi_i(R) = (-1)^{N+i}\sqrt{\frac{(1-x_i)}{R_0 x_i}}\,\frac{R\,P_N(2R/R_0 - 1)}{R - R_0 x_i}, \tag{23}$$

where $P_N(x)$ is the Legendre polynomial of degree N, and x_i are the zeros of $P_N(2x_i - 1) = 0$. This mesh is used for the scattering wave functions $\chi^{J\pi}_{L_A}(R)$ and $\chi^{J\pi}_{L_B}(R')$ and these basis functions satisfy the Lagrange conditions

$$\varphi_i(a x_j) = \frac{1}{\sqrt{R_0\lambda_i}}\delta_{ij}, \tag{24}$$

where λ_i are the weights of the Gauss-Legendre quadrature in the $[0, 1]$ interval.

For the bound state wave functions of nucleus A and B, where the interval range is $[0, \infty]$, the N Lagrange functions are chosen as

$$\varphi_i(R) = (-1)^i\frac{R}{R - x_i h}\frac{1}{\sqrt{x_i}}L_N(R/h)\exp(-R/2h), \tag{25}$$

where x_i are the roots of the Laguerre polynomials $L_N(x)$ and h is a scale parameter which is adapted to the typical dimensions of the system. In this case the Lagrange condition is given by

$$\varphi_i(h\,x_j) = \delta_{ij}/\sqrt{h\lambda_i}, \tag{26}$$

where λ_i are now the weights associated with the Gauss-Laguerre quadrature.

Using these functions, matrix elements of the overlap and of a local potential $V(r)$ then take the form

$$\begin{aligned}\langle\varphi_i|\varphi_j\rangle &\approx \delta_{ij}\\ \langle\varphi_i|V|\varphi_j\rangle &\approx V(R_0x_i)\delta_{ij} \text{ for Legendre functions}\\ &\approx V(hx_i)\delta_{ij} \text{ for Laguerre functions.}\end{aligned} \quad (27)$$

Similarly, one can get simpler expressions for the matrix elements of the kinetic energy and they are given in Ref. [26]. The upshot of using the Lagrange functions is that the value of the potential is required only at mesh points as evident from Eq. (27).

Finally, for a sufficient large channel radius, the transfer scattering matrix [Eq. (10)] in the combined R-matrix and Lagrange mesh approach, takes the simpler form

$$U^{J\pi}_{\alpha\beta} = -\frac{i\sqrt{SF_ASF_B}}{\hbar} \times R_0^3 \sum_{i,j=1}^{N} c_i^\alpha c_j^\beta \sqrt{\lambda_i\lambda_j}x_ix_jK^{J\pi}_{\alpha\beta}(R_0x_i,R_0x_j), \quad (28)$$

where coefficients c_i^α and c_j^β are associated with the scattering wave functions $\chi^{J\pi}_{L_A}(R)$ and $\chi^{J\pi}_{L_B}(R')$, respectively.

The number of basis functions has to be chosen large enough to ensure the convergence. As discussed in Ref. [22], typically $N \approx 30-40$ are sufficient to achieve the convergence and these are significantly lesser than the number of points (of the order of ~ 500) needed in finite-difference methods. In our approach, most of the computation time is consumed in the inversion of complex matrix $\boldsymbol{C}_L$ [Eq. (19)]. For a large channel radius one needs larger value of N to achieve the convergence and hence the size of matrix will be large. As bigger matrices need more time for inversion, so it can slow down the computations. However, this issue can be addressed by using the propagation techniques [33,24], where the interval $[0, R_0]$ is split into sub-intervals so that in each sub-interval one needs only reduced number of Lagrange functions and hence matrices sizes will be small. This procedure is beneficial when dealing with more complex situations like in case of large number of coupled equations.

Once we calculate the scattering matrices [Eq. (28)], the transfer cross sections can be computed from them (see, for example, Ref. [24,22]). The integrated transfer cross section is given by

$$\sigma_t = \frac{\pi}{k^2(2I_A+1)}\sum_J (2J+1)T_J, \quad (29)$$

with

$$T_J = \sum_\pi \sum_{L_A,I_B,L_B} |U^{J\pi}_{I_AL_A,I_BL_B}|^2. \quad (30)$$

3 Results and discussions

I now discuss our method using two test cases, one is of nucleon transfer and the other is of α transfer. In particular, I discuss the ^{16}O$(d,n)^{17}$F and ^{12}C(^{7}Li, $t)^{16}$O reactions at two different beam energies in each case. I initially focus on the uses of the R matrix and Lagrange mesh methods and discuss about the important parameters such as the channel radius R_0 and the number of basis functions N which are chosen to ensure the convergence of our results. Such tests were earlier performed in Ref. [22] in the context of ^{16}O$(d,p)^{17}$O reaction and here I discuss these briefly again while discussing the case of ^{16}O$(d,n)^{17}$F. I then discuss about the importance of the remnant term, peripheriality of the reaction, post-prior form equivalence and the effects of shallow potentials on the spectroscopic factors. Throughout this paper, I use integer masses, and the constant $\hbar^2/2m_N = 20.9$ MeV$\cdot fm^2$ (m_N is the nucleon mass).

Before I start discussing our results it is important to mention the various potentials used in the calculations to generate the bound and scattering states wave functions. For the bound-state calculations, we use potentials from the literature, mainly of Woods-Saxon type, which reproduce the binding energy of the concerned state. With central, Coulomb and spin-orbit terms, they are taken of the following form

$$\begin{aligned}V(r) &= -V_r\, f(r,R_r,a_r) + V_c(r)\\ &\quad - V_{so}\Big(\frac{\hbar}{m_\pi\, c}\Big)^2 \frac{1}{r}\frac{d}{dr} f(r,R_{so},a_{so})\boldsymbol{\ell\cdot s},\end{aligned} \quad (31)$$

where $f(r,R,a) = 1/[1+\exp(\frac{r-R}{a})]$. V_c is the Coulomb potential of an uniformly charged sphere with radius R_c and m_π is the pion mass.

The deuteron ground-state wave function (s state) on the other hand is calculated with the standard Gaussian potential

$$V_{np}(r) = -72.66\, \exp[-(r/1.484)^2]. \quad (32)$$

In Table 1, I give various parameters used in our calculations. In order to reproduce the experimental binding energies, the depths of the potentials are slightly adjusted as compared to those mentioned in the original references.

Table 1. Woods-Saxon potential parameters for bound states.

System	state	V_r (MeV)	R_r (fm)	a_r (fm)	V_{so} (MeV)	R_{so} (fm)	a_{so} (fm)	R_c (fm)
$p+^{16}$O[a]	$5/2^+$	47.68	3.34	0.5	10.30	3.34	0.5	3.28
	$1/2^+$	50.72	3.34	0.5	10.30	3.34	0.5	3.28
$\alpha+t$[b]	$3/2^-$	94.0	2.05	0.70				2.05
$\alpha+^{12}$C[b]	0^+_2	71.05	4.50	0.53				5.0
	2^+_1	69.15	4.50	0.53				5.0

[a] Ref. [34].
[b] Refs. [35,22].

The optical potentials used to calculate the scattering wave functions have the form

$$\begin{aligned}U(r) &= -V_r\, f(r,R_r,a_r) + V_c(r)\\ &\quad - i\,W_v\, f(r,R_v,a_v) - i\,W_s\, g(r,R_s,a_s),\end{aligned} \quad (33)$$

Table 2. Optical potential parameters defined by Eqs. (33 - 34), for the various channels involved in the reactions considered in this paper.

channel	$E_{\rm lab}$ (MeV)	V_r (MeV)	R_r (fm)	a_r (fm)	W_v (MeV)	R_v (fm)	a_v (fm)	W_s (MeV)	R_s (fm)	a_s (fm)	R_c (fm)	Ref.
d+^{16}O	7.73	109	2.52	0.80				5.10	4.79	0.60	3.28	[34]
	11	106	2.52	0.68				4.60	4.54	0.76	3.28	[34]
n+^{17}F	7.73, 11	47.0	3.15	0.65				6.0	3.15	0.47	3.34	[34][a]
^{7}Li+^{12}C	28, 34	139.1	3.71	0.58	18.8	4.56	0.93				2.91	[35]
t+^{16}O	28, 34	170	2.87	0.723	20	4.03	0.8				3.12	[35]
t+^{12}C	28	138.48	2.29	0.792	2.49	3.11	0.80	11.22	1.36	0.80	2.98	[36]
	34	134.41	2.31	0.792	2.76	3.11	0.80	10.92	1.36	0.80	2.98	[36]

[a] originally adopted from Ref. [37], where they were obtained at 14.3 MeV.

where the imaginary potential contains a volume term and a surface term defined by

$$g(r, R_s, a_s) = -4\, a_s \frac{d}{dr} f(r, R_s, a_s). \tag{34}$$

We mainly use the phenomenological optical potentials, unless otherwise mentioned, available in the literature and they were obtained by fitting elastic scattering data.

In Table 2, I give parameters of various optical potentials used for the ^{16}O$(d,n)^{17}$F and ^{12}C(^{7}Li, t)^{16}O reactions. For the ^{12}C(^{7}Li, t)^{16}O reaction they are same as given in Table II of Ref. [22] and were adopted from Refs. [35,36]. For the sake of simplicity, spin-orbit effects are neglected.

3.1 The ^{16}O$(d,n)^{17}$F reaction

I first start with the nucleon transfer case i.e. the ^{16}O(d,n) ^{17}F reaction and address the role of the R-matrix and Lagrange mesh parameters in our approach. I consider the transfer of a neutron to the ground $(5/2^+)$ and to the first excited state $(1/2^+, E_x = 0.495$ MeV) of ^{17}F at two different energies of deuteron $E_d = 7.73$ and 11 MeV. These states of ^{17}F are constructed by coupling the 0^+ ground state of ^{16}O with the neutron in $1d_{5/2}$ and $2s_{1/2}$ orbitals, respectively and I further assume a SF $= 1$ for both these states.

In Fig. 2, I plot the angular distributions of ^{16}O(d,n) ^{17}F reaction and compare them with the experimental data of Ref. [34]. Solid and dashed lines in the figure represent the calculations with and without the inclusion of the remnant term in the interaction (12). For these calculations, the ^{16}O $+ n$ optical potential is adopted from the global parametrization of Ref. [38]. Comparison of these two calculations allows us to study the importance of the remnant term in the ^{16}O$(d,n)^{17}$F reaction and for that I keep SFs equal to unity in Fig. 2. It is clear from the figure that both these calculations reproduce the shape of the data at forward angles, as normally expected in DWBA calculations. Furthermore, there is a significant difference at larger angles ($> 30^\circ$) in both these calculations. For the neutron transfer to the ground state (g.s.) of ^{17}F, even at

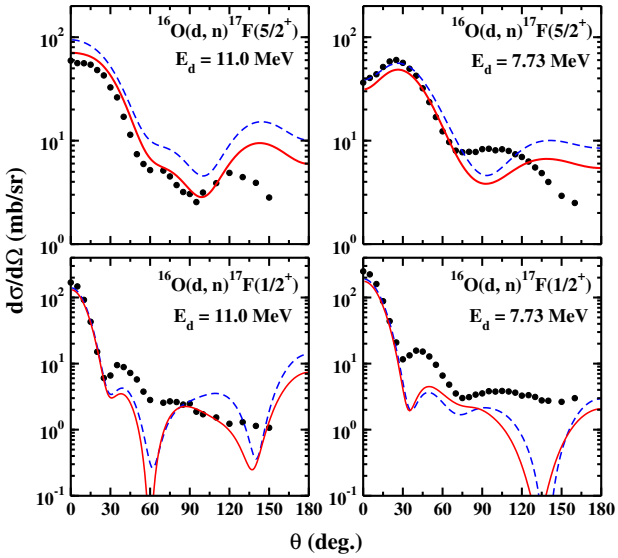

Fig. 2. Angular distributions of ^{16}O$(d,n)^{17}$F reaction for the ground $(5/2^+)$ and first excited $(1/2^+)$ states of ^{17}F at two deuteron energies. Solid and dashed lines correspond to the calculations (using SFs $= 1$) with and without the inclusion of the remnant term in the potential. Experimental data are taken from Ref. [34].

very forward angles this difference is around 30%. Such a large difference can influence the SFs extracted in the DWBA analysis. In Table 3, I give single particle SFs for the ground and the first excited states of ^{17}F, extracted at both these energies with and without the remnant term in the interaction. SFs are extracted by fitting the calculations to the experimental data up to the first minimum (normal way to extract SFs in the DWBA analysis [31]) using chi-square minimization fitting procedure. One can see that the inclusion of the remnant term in the interaction can change the extracted SFs. This change in the SFs is less than 10% for the excited state of ^{17}F, whereas, it is around $20 - 30\%$ for the ground state. I would like to mention here that, my goal in this paper is not to provide the optimal SFs but it is to estimate the effects of remnant term (and of the shallow potentials in the coming sections) on the SFs. As discussed in Ref. [34], around

$20-25\%$ uncertainties are expected in the extracted SFs, due to the ambiguities of the optical potentials.

Table 3. Single particle SFs for the ground and first excited states of ^{17}F and α-SFs for the 0^+_2 and 2^+_1 states of ^{16}O, extracted with and without the remnant terms (RT) in Eq. (12). The SFs for the ground state of d and of ^{7}Li are taken as 1. Uncertainties in the α-SFs of ^{16}O arise due to the variations of the angular range for the fits (see text).

Nucleus	State	Beam energy (MeV)	SFs without RT	SFs With RT
^{17}F	$5/2^+$	7.73	0.99	1.17
		11.0	0.63	0.81
^{17}F	$1/2^+$	7.73	1.26	1.38
		11.0	1.16	1.25
^{16}O	0^+_2	28	0.14 ± 0.02	0.18 ± 0.04
^{16}O	0^+_2	34	0.16 ± 0.02	0.24 ± 0.04
^{16}O	2^+_1	28	0.16 ± 0.02	0.17 ± 0.02
^{16}O	2^+_1	34	0.14 ± 0.02	0.16 ± 0.02

Now I analyze the sensitivity of the transfer cross section against variations of the R-matrix parameters: the channel radius R_0 and the number of basis functions N. For this, in Fig. 3, I plot the $^{16}\mathrm{O}(d,n)^{17}\mathrm{F}(1/2^+)$ differential cross section at $E_d = 11$ MeV and $\theta = 2^\circ$ as a function of (a) the number of basis functions N, for a fixed value of $R_0 = 35$ fm and (b) of the channel radius R_0, for a fixed value of $N = 80$. As mentioned earlier, the channel radius has to be large enough so that the nuclear interactions become negligible. However, large values require large bases, and hence increase the computer times. Therefore, a compromise must be adopted for the R-matrix calculations.

Note that, in principle, after the application of R-matrix method, the integral in Eq. (10) should have two parts, the internal from 0 to R_0 and the external from R_0 to ∞. However, in our approach we have consider R_0 as large enough, so that the latter part contribute negligibly small and it is rejected while deriving Eq. (28). So therefore, the channel radius in our approach is also serving as an upper limit of the integral to ensure the convergence.

From Fig. 3(a) it is clear that $N \approx 40$ are sufficient to achieve a good convergence. In fact, these numbers are much smaller than those required in finite-difference methods, such as the Numerov algorithm where hundreds of points are needed with typical mesh size of 0.02 fm. Fig. 3(b) shows that channel radii of around 25 fm and 35 fm are required to achieve the convergence respectively for the ground and for the first excited states of ^{17}F. A large radius needed in case of $1/2^+$ state is due to its loosely bound nature. In Fig. 4, the angular distribution for the n transfer leading to the ground state of ^{17}F at $E_d = 11$ MeV is plotted as a function of R_0 for a fixed value of number of basis functions, $N = 80$. This also confirms the findings of Fig. 3(b) i.e. the convergence is achieved for $R_0 \approx 20 - 25$ fm. Similar calculations were performed in

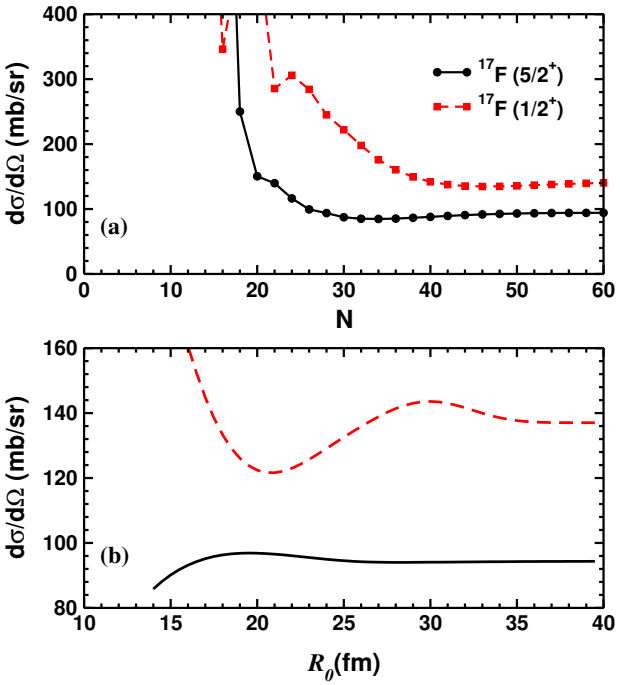

Fig. 3. $^{16}\mathrm{O}(d,n)^{17}\mathrm{F}(1/2^+)$ transfer cross section at $E_d = 11$ MeV and $\theta = 2^\circ$ as a function of the number of basis functions N (a) and of the channel radius (b).

Ref.[22] for the $^{16}\mathrm{O}(d,p)^{16}\mathrm{O}$ reaction, where $R_0 = 15-20$ fm was found as large enough to achieve the convergence, which is also true for the $^{12}\mathrm{C}(^7\mathrm{Li},\, t)^{16}\mathrm{O}$ reaction.

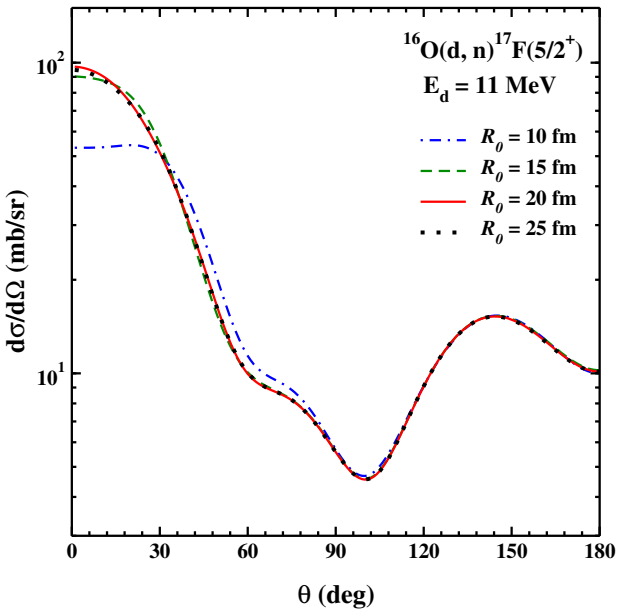

Fig. 4. $^{16}\mathrm{O}(d,n)^{17}\mathrm{F}$ transfer cross section to the ground state of ^{17}F at $E_d = 11$ MeV for various channel radii.

3.2 The ^{12}C(^{7}Li, t)^{16}O reaction

I now discuss the case of cluster transfer i.e. the ^{12}C(^{7}Li, t)^{16}O reaction, where an α cluster is transferred from the projectile ^{7}Li to the C target. In the literature α transfer reactions over the ^{12}C such as (^{7}Li, t) and (^{6}Li, d), have been used in many indirect measurements of the ^{12}C(α, γ)^{16}O cross section (see for example [35,39]) which is an important astrophysical reaction. Apart from determining the C/O abundance ratio after the Helium burning stage, it also decides the fate of the stars after their death through supernova explosion.

At stellar energies of interest ($\approx$ 300) keV the cross sections of ^{12}C(α, γ)^{16}O reaction are too small to be measured in the laboratory. Although many direct measurements have been performed to study this reaction but the cross sections down to 300 keV are still reliable on the extrapolation procedure and are uncertain (see for example [40]). Most fits of the available data are performed within the phenomenological R-matrix theory, which involves various parameters (such as energies, widths etc.) of ^{16}O states. It is well known that the reduced α widths of bound states are proportional to the SFs or to the ANCs and therefore, α transfer reactions such as (^{7}Li, t) and (^{6}Li, d) provide an efficient way to determine them.

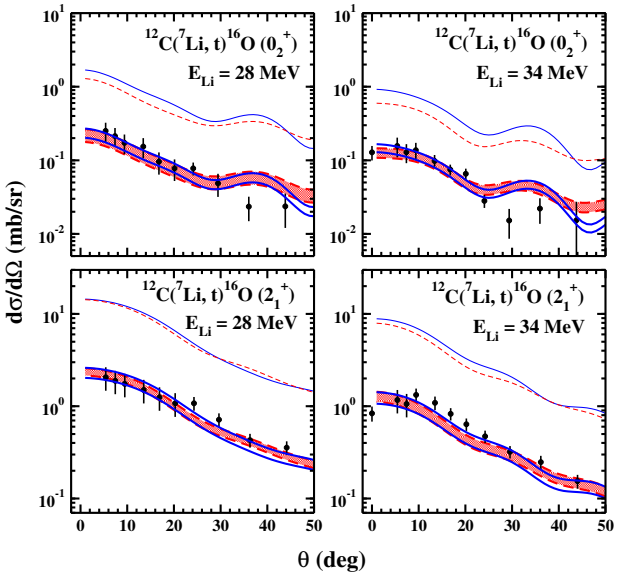

Fig. 5. Angular distributions of ^{12}C(^{7}Li, t)^{16}O reaction at two different energies of ^{7}Li. Dashed and solid line are calculations with and without the remnant terms, respectively. Thin lines (solid as well as dashed) correspond to the calculations when SFs are taken as 1, whereas thick lines are calculations using α-SFs given in the Table 3. Experimental data (solid dots) are taken from Ref. [35]. The hatched regions and upper and lower limits, represent the uncertainties associated with the angular range. For details see text.

I consider the α transfer leading to the 0_2^+ (E_x = 6.05 MeV) and 2_1^+ (E_x = 6.92 MeV) states of ^{16}O at two different energies of ^{7}Li, which are taken as 28 and 34 MeV, respectively. In order to reproduce the α separation energies, the depths of the potentials are adjusted (as given in Table 1) considering that the number of nodes n satisfies the condition $2n + \ell = 8$, where $\ell = 0$ and 2 for the 0_2^+ and 2_1^+ states, respectively. Similar to the previous case, calculations are performed with and without the remnant terms in the interaction. For this the $t-^{12}$C potentials are adopted from Ref. [36]. In Fig. 5, I plot the angular distributions of ^{12}C(^{7}Li, t)^{16}O reaction and compare them with the experimental data of Ref. [35]. Dashed and solid lines in the figure represent the calculations with and without the remnant terms, respectively. Thin lines (solid as well as dashed) correspond to the calculations when SFs are taken as 1, whereas the bands (hatched regions, upper and lower limits) are calculations using the extracted α-SFs given in the table 3. These SFs are extracted by normalizing the calculations to the data, using the chi-square minimization fitting procedure. However, as there is no clear minima in the data like in the previous case, I fit the data in steps with an increment of 10° and extract the SFs in each interval. This procedure we have adopted in Ref. [23] where, the average of all these SFs obtained in different intervals gives the final SF of a given state. This also brings additional uncertainties in the extracted SFs along with the existing uncertainties due to the optical potentials, which are around 46% and 33% (see Ref. [35]) for 0_2^+ and 2_1^+ states, respectively. The extracted α SFs in table 3 are nearly the same as those obtained in Ref. [35] where they were reported as $0.13^{+0.07}_{-0.06}$ and 0.15 ± 0.05, respectively for the 0_2^+ and 2_1^+ state of ^{16}O. With remnant terms in the interaction, SFs for the 2_1^+ state slightly increase by around $6-14$%, whereas for the 0_2^+ state there is an increase of around $30-50$% in their values and this was also pointed out in Ref [22]. Moreover, in Ref. [22], we have also repeated our calculations with another $t-^{12}$C potentials from Ref. [41] and confirmed that our results remain nearly same.

3.3 Post-prior equivalence

Next I discuss the post-prior form equivalence in the context of examples considered here. In fact, post-prior equivalence is well known and had been discussed in some textbooks, see for example [31], where it is shown that in the DWBA, the post and the prior forms give same results provided the remnant terms are included in the interaction. Here I show it explicitly by performing calculations with and without the remnant terms.

In Fig. 6, I plot the angular distributions of (a) ^{16}O(d, n) ^{17}F($5/2^+$) at E_d = 11 MeV and of (b) ^{12}C(^{7}Li, t)^{16}O(0_2^+) at $E_{\rm Li}$ = 28 MeV. Dashed and dot-dashed lines represent calculations in the post and the prior forms, respectively without the remnant terms in the interactions (12) and (13). Whereas, solid and dotted lines represent calculations in the post and prior forms, respectively including the remnant terms. One can see that, both representations give almost same results only when remnant terms are included in the interactions in both these cases. Similar, results were obtained for the other states and energies

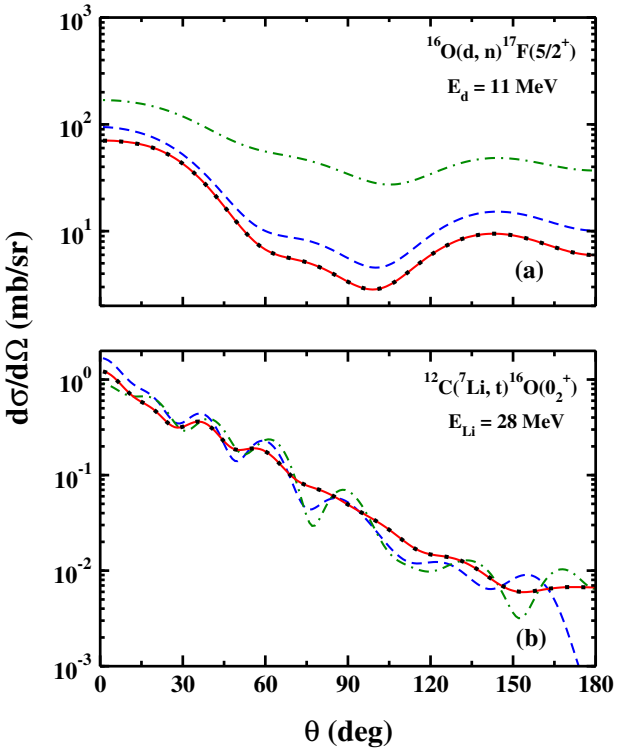

Fig. 6. Angular distribution of (a) $^{16}\mathrm{O}(d,n)^{17}\mathrm{F}(5/2^+)$ at $E_d = 11$ MeV and of (b) $^{12}\mathrm{C}(^7\mathrm{Li},t)^{16}\mathrm{O}(0_2^+)$ at $E_{Li} = 28$ MeV in the DWBA framework. Dashed and dot-dashed lines represent the calculations in the post and prior forms, respectively without the remnant terms in the interactions (12) and (13). Whereas, solid and dotted lines represent the calculations in the post and prior forms, respectively including the remnant terms.

in both these reactions. Furthermore, in Fig. 6 (a) one can see that the post form calculations without the remnant term (dashed line) are closer to the calculations with the remnant term (solid and dotted lines) regarding the shape as well as the magnitude. This is again due to the similar magnitude of the $n-^{16}$O and $n-^{17}$F optical potentials and somewhat justify the post form DWBA calculations without the remnant terms in case of (d,p) and (d,n) reactions.

3.4 Test of the peripherality

Transfer reactions are assumed peripheral for energies below the barrier and even above it. This means the contributions to the reaction cross section from the nuclear interior are small or in other words, reaction probes the long-range part of the wave function. In this region the bound state wave function behaves like Whittaker function

$$u_\ell^I(r) \longrightarrow C_\ell^I\, W_{-\eta,\ell+1/2}(2\kappa r), \tag{35}$$

where η and κ are the Sommerfeld parameter and bound state wave number, respectively and C_ℓ^I is the ANC of the concerned bound state.

In fact, DWBA calculations of the peripheral transfer reactions are widely used to determine the ANCs by comparing them with the data [12]. Peripherality of the reaction has been addressed, for example in Refs. [12,42]. However, assessing the peripherality of transfer reaction is not trivial. This can be understood by looking at the transfer kernel [Eq. (11)] which depends on the R and R' i.e. the relative coordinates of the colliding nuclei, whereas the peripheral character of the reaction is associated with the internal coordinates r_A and r_B (see Fig. 1).

To address this issue and to analyze the peripheral nature of a transfer reaction, in Ref. [22] using a cutoff radius r_{min} over r_A or r_B, we defined a modified kernel as

$$\begin{aligned}\tilde{K}^{J\pi}_{\alpha\beta}(r_{min},R,R') &= K^{J\pi}_{\alpha\beta}(R,R') \text{ for } r_{min} \le r_A \text{ or } r_B\\ &= 0 \text{ for } r_{min} > r_A \text{ or } r_B.\end{aligned} \tag{36}$$

This definition then leads to the modified scattering matrix, given by

$$\begin{aligned}\tilde{U}^{J\pi}_{\alpha\beta}(r_{min}) = -\frac{i}{\hbar}\int \chi^{J\pi}_{L_A}(R)\tilde{K}^{J\pi}_{\alpha\beta}(r_{min},R,R')\chi^{J\pi}_{L_B}(R')\\ \times RR'dRdR',\end{aligned} \tag{37}$$

such that

$$\begin{aligned}\tilde{U}^{J\pi}_{\alpha\beta}(0) &= U^{J\pi}_{\alpha\beta}\\ \tilde{U}^{J\pi}_{\alpha\beta}(\infty) &= 0.\end{aligned} \tag{38}$$

If a process is peripheral then one can expects a significant value of $\tilde{U}^{J\pi}_{\alpha\beta}(r_{min})$ for large value of r_{min}, on the other hand, if $\tilde{U}^{J\pi}_{\alpha\beta}(r_{min})$ rapidly tends to zero, then the process can be considered as internal.

Note that the peripheral nature depends on the angular momentum and this we have verified in Ref. [22] We have shown that for higher J values, reaction is more peripheral as compared to the low J values which mostly depend on the internal contributions. In Ref. [22], we have discussed the peripherality of the $^{16}\mathrm{O}(d,p)^{17}\mathrm{O}$ and $^{12}\mathrm{C}(^7\mathrm{Li},t)^{16}\mathrm{O}$ reactions and here I discuss the case of $^{16}\mathrm{O}(d,n)^{17}\mathrm{F}$.

In Fig. 7, I plot the modified scattering matrix (37) for the $^{16}\mathrm{O}(d,n)^{17}\mathrm{F}(g.s.)$ reaction at $E_d = 11$ MeV. For a given J, I have selected $L_B = |J - S_B|$, where $S_B = 2$, but the similar behavior was found for the other quantum numbers. From Fig. 7(a), one can see that for $p+n$ distances of > 2 fm, contributions to the scattering matrix are negligible. Same behavior was found in Ref. [22] for the $^{16}\mathrm{O}(d,p)^{17}\mathrm{O}$ reaction, which justify the zero-range approximation often used for the (d,p) and (d,n). Fig. 7(b) on the other hand confirms our previous findings about the peripheral nature of various partial waves. It is clear that higher partial waves are more peripheral than the lower ones.

From the different behavior of various J values, one can expect that the peripheral nature of the transfer cross section depends on the angle. This can be seen in Fig. 8, where I have plotted the modified cross sections [computed with the modified scattering matrices (37)] of the $^{16}\mathrm{O}(d,n)^{17}\mathrm{F}(g.s.)$ reaction at $E_d = 11$ MeV as a function

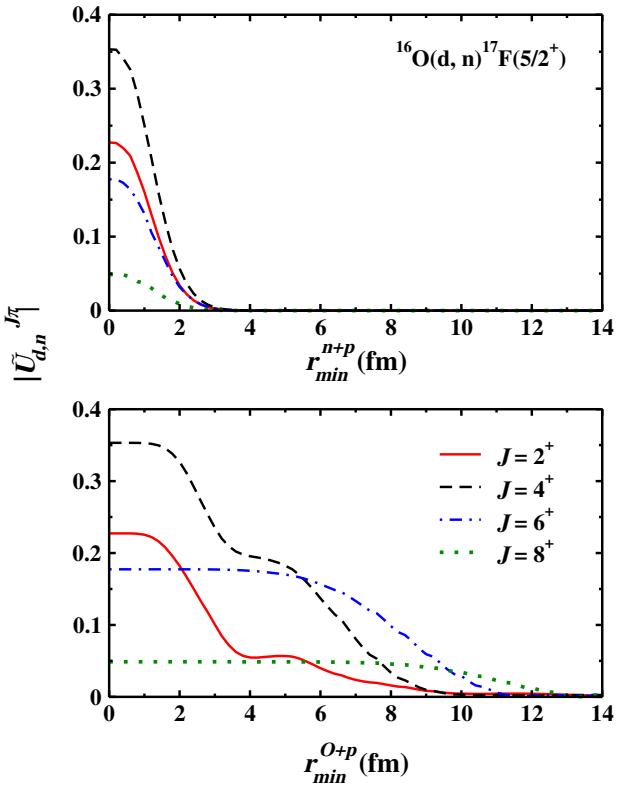

Fig. 7. Modulus of the modified scattering matrix $\tilde{U}^{J\pi}$ (37) for the ^{16}O$(d,n)^{17}$F$(g.s.)$ reaction at $E_d = 11$ MeV. The minimum distance r_{min} corresponds to the $p+n$ coordinate in panel (a) and to the p+^{16}O coordinate in panel (b).

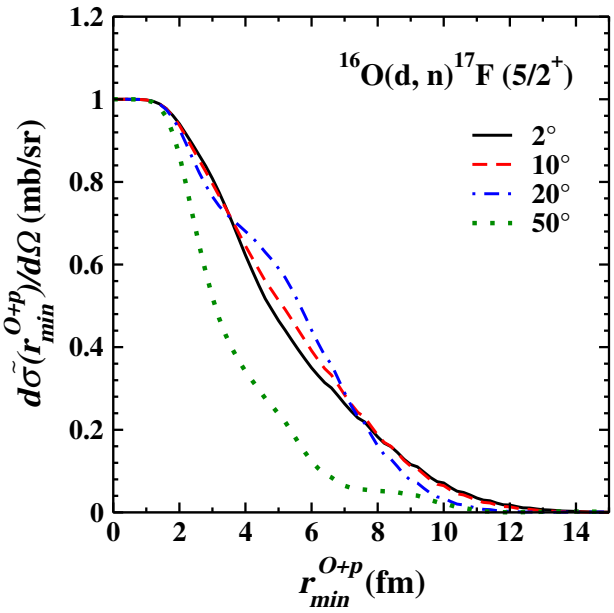

Fig. 8. Modified scattering cross sections $d\tilde{\sigma}(r_{min})/d\Omega$ for the ^{16}O$(d,n)^{17}$F$(g.s.)$ reaction at $E_d = 11$ MeV, and for different scattering angles. All curves are normalized to their values at $r^{O+p}_{min} = 0$.

of r_{min} for four different angles. All curves are normalized to their values at $r^{O+p}_{min} = 0$. It is clear from the figure that at small angles cross sections are more peripheral as compared to the large angles.

3.5 Effects of supersymmetric bound state potentials

I now discuss the effects of bound state potentials on the transfer cross sections in the DWBA framework. In spite of modern advancements in the reaction theory [18,19, 29,43–45], due to its simplicity DWBA is still being used in many experimental analysis, especially to extract the SFs or the ANCs (see for example [46–48]). However, the extracted SFs can contain uncertainties due to the ambiguities in the optical potentials. To minimize these uncertainties, the phenomenological optical potentials which fit the elastic scattering data at the reaction energies are preferred and in case such data are unavailable, especially for the exotic nuclei, simultaneous measurements of the elastic and transfer cross sections serve as ideal choice [49–51]. On the other hand, for the bound states, the two-body potentials such as Woods-Saxon (WS) or Gaussian type are mainly used with their parameters chosen to reproduce the experimental binding energies of the participating clusters, the usual separation energy prescription. However, different sets of these parameters can lead to different cross sections and hence the extracted SFs (see for example [42]). Moreover, two-body potentials constructed in this way for these many-body systems may contain Pauli-forbidden states, which are unphysical and also simulate the missing antisymmetrization effects. Such states do not exist in the fully microscopic calculations.

On the other hand, by performing the supersymmetric transformations [52,53] one can obtain the supersymmetric (SUSY) partner potentials without these deep states. The resultant ℓ-dependent potentials are usually shallow in nature with a repulsive core [53] and at positive energies, they give the same phase shifts. The wave functions obtained from these potentials also differ in the nuclear interior and possess a nodeless structure, however, in the exterior region they remain the same as those obtained from the deep potentials. In spite of these differences, both these wave functions (from shallow SUSY and deep WS potentials), give the similar spectroscopic properties such as root mean square (r.m.s) radii [54].

In Ref. [23], we studied the sensitivity of the transfer cross section to the bound state wave functions by using WS and its SUSY partner potentials. In fact, in the supersymmetric quantum mechanics, a Hamiltonian H_0 given by

$$H_0 = -\frac{\hbar^2}{2\mu}\frac{d^2}{dr^2} + V_0^{\ell j}(r), \tag{39}$$

can be transformed to its partner Hamiltonian H_2 by performing couple of transformations [53], which change the potential to $V_2^{\ell j}$, given by

$$V_2^{\ell j}(r) = V_0^{\ell j}(r) - \frac{\hbar^2}{\mu}\frac{d^2}{dr^2}\log\int_0^r |u_0(s)|^2 ds, \tag{40}$$

where μ is the reduced mass and potential $V_0^{\ell j}$ (WS type in our case) contains all the spin-orbit, centrifugal and Coulomb terms. $u_0(r)$ is the radial bound state wave function corresponding to the potential $V_0^{\ell j}$. The Hamiltonian H_2 obtained in this way, possess the identical energy spectrum to those of H_0, except for the lowest states which are suppressed [52,53]. With repeated applications of this procedure one can remove all the unphysical states from the spectrum of the parent Hamiltonian H_0. We apply these transformations to the bound state potentials in both the channels to remove all the forbidden states, which are given by a parity dependent limit N, so that states having principle quantum number $2n + \ell < N$ are forbidden.

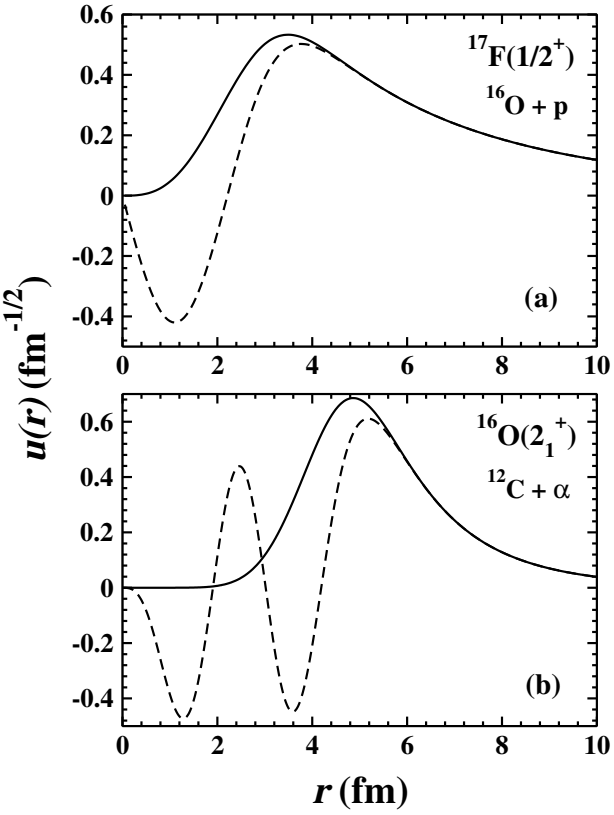

Fig. 9. Radial bound-state wave functions of ^{17}F$(1/2^+)$ and ^{16}O(2_1^+) obtained by solving the Schrödinger wave equation with the WS potentials (dashed lines) and with the SUSY potentials (solid lines).

In Fig. 9, I plot the radial bound state wave functions for the ^{17}F$(1/2^+)$ and ^{16}O(2_1^+) states for which the WS potentials given in Table 1 have respectively 1 and 3 Pauli-forbidden states. Dashed lines represent the wave functions obtained with the WS potentials, whereas solid lines are the wave functions obtained with the SUSY partner potentials generated with the above mentioned procedure. These two different combination of potentials and wave functions are used to calculae the transfer cross sections for the reactions under consideration.

I first consider the case of ^{16}O$(d,n)^{17}$F$(1/2^+)$, where there are 0 and 1 forbidden states correspond to $\ell = 0$ in

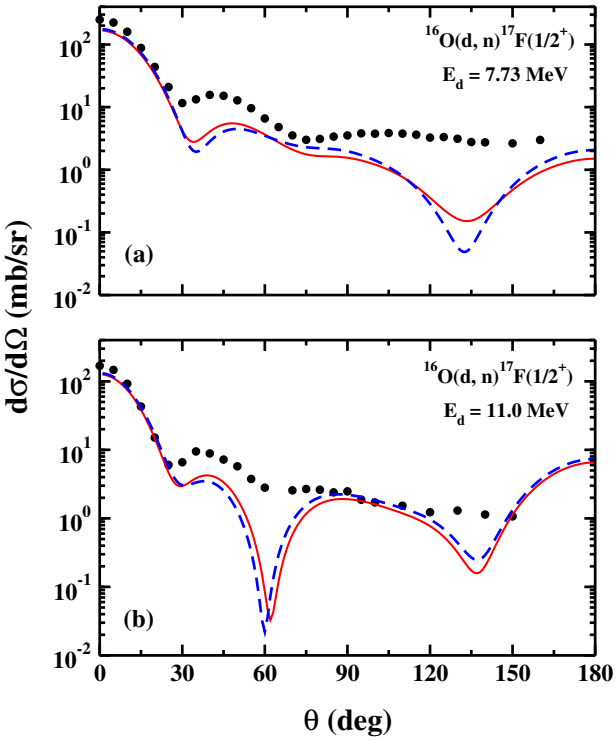

Fig. 10. ^{16}O$(d,n)^{17}$F$(1/2^+)$ angular distribution at two different deuteron energies. The dashed and solid lines correspond to the calculations (with SF = 1) using a WS and its SUSY partner for the ^{17}F$(1/2^+)$, respectively. Experimental data (solid dots) are taken from Ref. [34].

the initial and final channel bound state potentials, respectively. Note that for the ^{17}F$(5/2^+)$, there is no forbidden state in the potential, so p transfer leading to the ground state of ^{17}F is not considered here. In Fig. 10, I plot the angular distribution for the ^{16}O$(d,n)^{17}$F$(1/2^+)$ reaction at two different beam energies. The dashed and solid lines are calculations using a WS (given in Table 1) and its SUSY partner potential for the ^{17}F$(1/2^+)$, respectively. At both these energies, one can see that both calculations give nearly same results at forward angles whereas at higher angles they differ somewhat. This suggests, a negligible effect on the extracted SFs as one can see in Table 4. Using the SUSY potential for the ^{17}F$(1/2^+)$ state, the extracted SFs are changed by just 5%. This was expected at such a low energy, where the process is considered as peripheral at forward angles and also due to very small separation energy of ^{17}F$(1/2^+)$, most of the contributions to the cross sections come from larger distances.

Next, I consider the α transfer reaction ^{12}C$(^7$Li, $t)^{16}$O, which we have studied in detail in Ref. [23] and consider both the 0_2^+ and 2_1^+ states of ^{16}O. In this case, there is 1 Pauli-forbidden state for $\ell = 1$ in the $\alpha + t$ WS potential in the initial channel and there are respectively, 4 and 3 forbidden states for $\ell = 0$ and $\ell = 2$ in the final channel WS potentials for the 0_2^+ and 2_1^+ states of ^{16}O [23]. Therefore, in this case SUSY transformations are used to remove these forbidden states from both the channels. Fig. 11 shows the angular distributions of ^{12}C$(^7$Li, $t)^{16}$O reac-

Table 4. Single particle SFs for $1/2^+$ state of ^{17}F and α-SFs (adopted from Ref.[23]) for 0^+_2 and 2^+_1 states of ^{16}O extracted using two different types of bound-state potentials. The SFs for the ground state of d and of ^{7}Li are taken as 1.

Nucleus	State	Beam energy (MeV)	SFs (WS)	SFs (SUSY)
^{17}F	$1/2^+$	7.73	1.38	1.46
		11.0	1.25	1.31
^{16}O	0^+_2	28	0.18 ± 0.04	0.19 ± 0.02
^{16}O	0^+_2	34	0.24 ± 0.04	0.25 ± 0.03
^{16}O	2^+_1	28	0.17 ± 0.02	0.15 ± 0.02
^{16}O	2^+_1	34	0.16 ± 0.02	0.14 ± 0.03

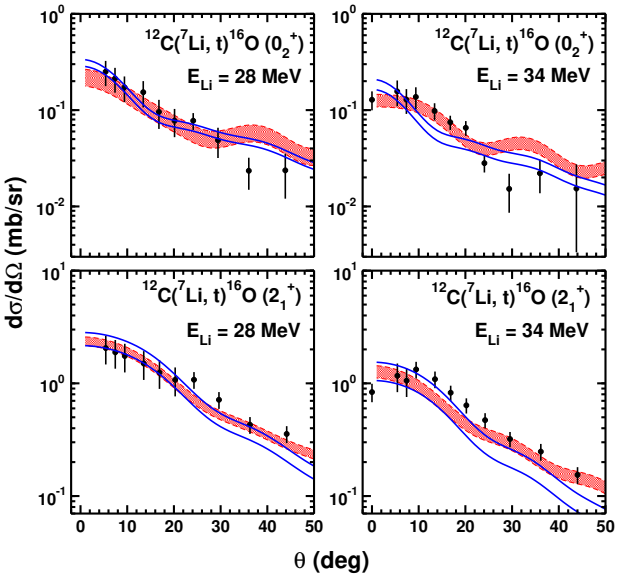

Fig. 11. Angular distributions of ^{12}C(^{7}Li, t)^{16}O at two ^{7}Li energies. Dashed (same as in Fig. 5) and solid lines represent calculations using WS and SUSY bound-state potentials in both channels, respectively. Experimental data are taken from Ref. [35]. Spectroscopic factors are given in Table 4. The upper and lower limits, and the hatched regions, represent uncertainties associated with the angular range (see text). Reprinted from Ref. [23].

tion at 28 and 34 MeV for both the states of ^{16}O. Dashed and solid lines represent calculations with the WS and the SUSY potential, respectively including remnant terms and they are fitted to the experimental data of Ref. [35] using the chi-square minimization procedure we have followed in Section 3.2. The uncertainties associated with the angular range are represented with the hatched regions for the dashed lines and the upper-lower limits for the solid lines.

The extracted α-SFs are given in Table 4. One can see that, α-SFs for the states of ^{16}O remain almost unchanged when we replace the WS potentials in both the channels by their respective SUSY partners. On the other hand, shapes of angular distributions are changed significantly (see Fig. 11). To further understand these shape changes, in Ref. [23] we have studied the variation of modified cross sections [computed with the modified scattering matrix Eq. (37)] as a function of cutoff radius over both the $\alpha+t$ and the $^{12}\mathrm{C}+\alpha$ distances. It was found that at larger angles where shapes of angular distributions are mostly affected, cross sections are mainly governed by $^{12}\mathrm{C}+\alpha$ distances. Whereas, at forward angles cross sections are equally sensitive to the $\alpha+t$ and $^{12}\mathrm{C}+\alpha$ distances. For more details one is refereed to Ref. [23]

Although in both these reactions considered here, the SFs are not affected much when SUSY potentials are used in place of WS, but in Ref. [23], we observed around 30% decrease in the SF for the first excited state of ^{17}O extracted using the $^{16}\mathrm{O}(d,p)^{17}\mathrm{O}$ reaction.

4 Summary

I have presented a short review of our recent work on cluster transfer reactions where we have applied the R-matrix and the Lagrange-mesh methods in the DWBA framework. To discuss applications of our approach I have considered $^{16}\mathrm{O}(d,n)^{17}\mathrm{F}$ and ^{12}C(^{7}Li, t)^{16}O reactions, which are typical cases of nucleon and α transfer. Sensitivity of transfer cross sections to the R-matrix parameters is discussed and it is found that only a small number of basis $\sim 40-50$, much smaller than in finite-difference methods, are sufficient to achieve the convergence. Apart from discussing the importance of the remnant terms and their effects on the extracted SFs, I have discussed the post-prior form equivalence in the DWBA and also the peripherality of transfer reactions with respect to the internal coordinates of the projectile as well as of the residual nucleus. Finally, supersymmetric partners of the bound state WS potentials which give wave functions with same asymptotics but differ in the nuclear interior, are used. Comparison of transfer calculations using both these bound state potentials and corresponding wave functions allows us to test the sensitivity of transfer cross sections to the nuclear interior. Subsequently, the effects of SUSY potentials on the extracted single particle and α-SFs are also studied. Although the shapes of angular distributions are affected to some extent, especially for the ^{12}C(^{7}Li, t)^{16}O reaction, the extracted SFs for the states of residual nuclei in both the reactions considered here, remain almost same.

Acknowledgments

This work has received funding from the European Union's Horizon 2020 research and innovation program under the Marie Skłodowska-Curie grant agreement No 801505. Author also thanks Pierre Descouvemont for fruitful comments and discussions.

References

1. P. Hodgson, E. Běták, Phys. Rep. **374**, 1 (2003)

2. M.S. Hussein, Ann. Phys. **90**, 48 (1975)
3. M.S. Hussein, Eur. Phys. J. A **53**, 110 (2017)
4. C.A. Bertulani, L.F. Canto, M.S. Hussein, Shubhchintak, T.V. Nhan Hao, Int. J. Mod. Phys. E **28**, 1950109 (2019)
5. G.R. Satchler, *Direct Nuclear Reactions* (Oxford University Press, 1983)
6. N. Glendenning, *Direct Nuclear Reactions* (World Scientific, Singapore, 2004)
7. T. Ohmura, B. Imanishi, M. Ichimura, M. Kawai, Progress of Theoretical Physics **41**, 391 (1969)
8. I.J. Thompson, Comput. Phys. Rep. **7**, 167 (1988)
9. A.M. Mukhamedzhanov, Shubhchintak, C.A. Bertulani, T.V.N. Hao, Phys. Rev. C **95**, 024616 (2017)
10. D.W. Bardayan, J. Phys. G: Nucl. Part. Phys. **43**, 043001 (2016)
11. C. Bertulani, Shubhchintak, A. Mukhamedzhanov, A.S. Kadyrov, A. Kruppa, D.Y. Pang, J. Phys.: Conf. Ser. **703**, 012007 (2016)
12. R.E. Tribble, C.A. Bertulani, M.L. Cognata, A.M. Mukhamedzhanov, C. Spitaleri, Rep. Prog. Phys. **77**, 106901 (2014)
13. C.A. Gagliardi, R.E. Tribble, A. Azhari, H.L. Clark, Y.W. Lui, A.M. Mukhamedzhanov, A. Sattarov, L. Trache, V. Burjan, J. Cejpek et al., Phys. Rev. C **59**, 1149 (1999)
14. J.S. Thomas, D.W. Bardayan, J.C. Blackmon, J.A. Cizewski, U. Greife, C.J. Gross, M.S. Johnson, K.L. Jones, R.L. Kozub, J.F. Liang et al., Phys. Rev. C **71**, 021302 (2005)
15. A.M. Mukhamedzhanov, F.M. Nunes, P. Mohr, Phys. Rev. C **77**, 051601 (2008)
16. R.C. Johnson, P.J.R. Soper, Phys. Rev. C **1**, 976 (1970)
17. N. Austern, Y. Iseri, M. Kamimura, M. Kawai, G. Rawitscher, M. Yahiro, Phys. Rep. **154**, 125 (1987)
18. A. Deltuva, Phys. Rev. C **88**, 011601 (2013)
19. E.O. Alt, L.D. Blokhintsev, A.M. Mukhamedzhanov, A.I. Sattarov, Phys. Rev. C **75**, 054003 (2007)
20. N.J. Upadhyay, A. Deltuva, F.M. Nunes, Phys. Rev. C **85**, 054621 (2012)
21. Y.H. Song, Y. Kim, J. Korean Phys. Soc. **73**, 1247 (2018)
22. Shubhchintak, P. Descouvemont, Phys. Rev. C **100**, 034611 (2019)
23. Shubhchintak, P. Descouvemont, Phys. Lett. B **811**, 135874 (2020)
24. P. Descouvemont, D. Baye, Rep. Prog. Phys. **73**, 036301 (2010)
25. P. Descouvemont, Comput. Phys. Commun. **200**, 199 (2016)
26. D. Baye, Phys. Rep. **565**, 1 (2015)
27. T. Tamura, Phys. Rep. **14C**, 59 (1974)
28. M. Gómez-Ramos, A.M. Moro, J. Gómez-Camacho, I.J. Thompson, Phys. Rev. C **92**, 014613 (2015)
29. A.M. Moro, F.M. Nunes, R.C. Johnson, Phys. Rev. C **80**, 064606 (2009)
30. J. Lei, A.M. Moro, Phys. Rev. C **97**, 011601 (2018)
31. I. Thompson, F. Nunes, *Nuclear Reactions for Astrophysics: Principles, Calculation and Applications of Low-Energy Reactions* (Cambridge University Press, 2009)
32. C. Bloch, Nucl. Phys. **4**, 503 (1957)
33. K.L. Baluja, P.G. Burke, L.A. Morgan, Comput. Phys. Commun. **27**, 299 (1982)
34. C. Oliver, P. Forsyth, J. Hutton, G. Kaye, J. Mines, Nucl. Phys. A **127**, 567 (1969)
35. N. Oulebsir, F. Hammache, P. Roussel, M.G. Pellegriti, L. Audouin, D. Beaumel, A. Bouda, P. Descouvemont, S. Fortier, L. Gaudefroy et al., Phys. Rev. C **85**, 035804 (2012)
36. D.Y. Pang, W.M. Dean, A.M. Mukhamedzhanov, Phys. Rev. C **91**, 024611 (2015)
37. V. Valković, G. Paić, I. Šlaus, P. Tomaš, M. Cerineo, G.R. Satchler, Phys. Rev. **139**, B331 (1965)
38. A.J. Koning, J.P. Delaroche, Nucl. Phys. A **713**, 231 (2003)
39. F.D. Becchetti, E.R. Flynn, D.L. Hanson, J.W. Sunier, Nucl. Phys. A **305**, 293 (1978)
40. R.J. deBoer, J. Görres, M. Wiescher, R.E. Azuma, A. Best, C.R. Brune, C.E. Fields, S. Jones, M. Pignatari, D. Sayre et al., Rev. Mod. Phys. **89**, 035007 (2017)
41. X. Li, C. Liang, C. Cai, Nucl. Phys. A **789**, 103 (2007)
42. D.Y. Pang, F.M. Nunes, A.M. Mukhamedzhanov, Phys. Rev. C **75**, 024601 (2007)
43. N.B. Nguyen, F.M. Nunes, R.C. Johnson, Phys. Rev. C **82**, 014611 (2010)
44. K.T. Schmitt, K.L. Jones, S. Ahn, D.W. Bardayan, A. Bey, J.C. Blackmon, S.M. Brown, K.Y. Chae, K.A. Chipps, J.A. Cizewski et al., Phys. Rev. C **88**, 064612 (2013)
45. D. Walter, S.D. Pain, J.A. Cizewski, F.M. Nunes, S. Ahn, T. Baugher, D.W. Bardayan, T. Baumann, D. Bazin, S. Burcher et al., Phys. Rev. C **99**, 054625 (2019)
46. V. Srivastava, C. Bhattacharya, T.K. Rana, S. Manna, S. Kundu, S. Bhattacharya, K. Banerjee, P. Roy, R. Pandey, G. Mukherjee et al., Phys. Rev. C **91**, 054611 (2015)
47. H. Jayatissa, G. Rogachev, V. Goldberg, E. Koshchiy, G. Christian, J. Hooker, S. Ota, B. Roeder, A. Saastamoinen, O. Trippella et al., Phys. Lett. B **802**, 135267 (2020)
48. C.B. Hamill, P.J. Woods, D. Kahl, R. Longland, J.P. Greene, C. Marshall, F. Portillo, K. Setoodehnia, Eur. Phys. J. A **56**, 36 (2020)
49. A. Strömich, B. Steinmetz, R. Bangert, B. Gonsior, M. Roth, P. von Brentano, Phys. Rev. C **16**, 2193 (1977)
50. K.T. Schmitt, K.L. Jones, A. Bey, S.H. Ahn, D.W. Bardayan, J.C. Blackmon, S.M. Brown, K.Y. Chae, K.A. Chipps, J.A. Cizewski et al., Phys. Rev. Lett. **108**, 192701 (2012)
51. R. Wolski, A. Fomichev, A. Rodin, S. Sidorchuk, S. Stepantsov, G. Ter-Akopian, M. Chelnokov, V. Gorshkov, A. Lavrentev, Y. Oganessian et al., Phys. Lett. B **467**, 8 (1999)
52. C.V. Sukumar, J. Phys. A: Math. Gen. **18**, 2917 (1985)
53. D. Baye, Phys. Rev. Lett. **58**, 2738 (1987)
54. D. Ridikas, J. Vaagen, J. Bang, Nucl. Phys. A **609**, 21 (1996)